ELSEVIER

Journal of Nuclear Materials 265 (1999) 308–320

journal of nuclear materials

Oxidation kinetics of hydride-bearing uranium metal corrosion products

Terry C. Totemeier *, Robert G. Pahl, Steven M. Frank

Argonne National Laboratory, Materials Characterization, Engineering Division, P.O. Box 2528, Idaho Falls, ID 83403-2528, USA

Received 27 July 1998; accepted 8 October 1998

Abstract

The oxidation behavior of hydride-bearing uranium metal corrosion products from Zero Power Physics Reactor (ZPPR) fuel plates was studied using thermo-gravimetric analysis (TGA) in environments of Ar–4%O_2, Ar–9%O_2, and Ar–20%O_2. Ignition of corrosion product samples from two moderately corroded plates was observed between 125°C and 150°C in all environments. The rate of oxidation above the ignition temperature was found to be dependent only on the net flow rate of oxygen in the reacting gas. Due to the higher net oxygen flow rate, burning rates increased with increasing oxygen concentration. Oxidation rates below the ignition temperature were much slower and decreased with increasing test time. The hydride contents of the TGA samples from the two moderately corroded plates, determined from the total weight gain achieved during burning, were 47–61 wt% and 29–39 wt%. Samples from a lightly corroded plate were not reactive; X-ray diffraction (XRD) confirmed that they contained little hydride.

1. Introduction

The reaction of uranium metal with water vapor has been extensively studied; several detailed reviews have been published [1–3]. The reaction nominally produces UO_2, according to the formula

$$U + 2H_2O \rightarrow UO_2 + 2H_2. \quad (1)$$

The oxide formed was found to be slightly superstoichiometric in an early study by Baker et al. [4], however, more recent studies [1,5–7] have reported the formation of stoichiometric UO_2. Some researchers also report the presence of uranium hydride, UH_3, in the reaction product. The reported values of the percentages of UH_3 in the reaction product vary [4,8–10]; the exact mechanism of hydride formation has not been conclusively identified. The formation of higher percentages of UH_3 appears to be limited to crevice-type corrosion where there is limited access of the ambient environment to the reaction product. UH_3 has also been observed to form as isolated inclusions in the metal phase of corroded metallic uranium spent nuclear fuel (SNF) [11].

The formation of UH_3 as a product of uranium corrosion by H_2O is a safety concern due to the reactivity of UH_3 at low temperatures. Pure UH_3, which forms as a fine powder, is reported to exhibit pyrophoric behavior in air [12]. An early report on U metal fires [13] concluded that UH_3 formation and reactivity plays a strong role in the initiation of metal fires. Despite this known hazard, few studies have been performed to fully characterize the reaction of hydride with oxygen. The reaction is known to produce U_3O_8 [12,14]:

$$3UH_3 + \frac{25}{4}O_2 \rightarrow U_3O_8 + \frac{9}{2}H_2O \quad (2)$$

and liberates a significant amount of heat, 1490 kJ/mol UH_3. A recent literature review of UH_3 properties with respect to uranium corrosion was performed by Robinson and Thomas [15].

Two quantitative studies of the reaction of UH_3 with O_2 and air were performed by Stakebake [16] and Longhurst [17] using thermo-gravimetric analysis (TGA). Stakebake performed oxidation tests on pure UH_3 prepared by reaction of U metal with H_2 (hydrid-

* Corresponding author.

0022-3115/99/$ – see front matter
PII: S0022-3115(98)00649-7

ing). Tests were performed in pure oxygen at 0°C, 50°C, and 100°C. Contrary to typical oxidation behavior, the rates observed were higher at 0°C and 50°C than at 100°C; the apparent anomaly was not explained. Longhurst also performed tests on pure UH_3 formed by hydriding. In these tests, air was introduced gradually to the hydride, with no immediate reaction. Subsequent heating of the UH_3 in air produced a vigorous reaction which began at 140°C. The heat generated by the reaction was sufficient to melt the Pt sample pan (melting temperature of 1772°C). The weight gain of the sample showed essentially a step function when the reaction occurred. No burning rate was reported.

Interest in the oxidation kinetics of UH_3 has been recently renewed due to the extended underwater storage of metallic SNF and the anticipated interim to long-term dry storage of SNF and uranium metal feedstock. The principal concern with such extended storage of uranium metal is degradation due to corrosion by H_2O (in both liquid and vapor forms) and the possibility of forming corrosion products containing UH_3. Information on the behavior of UH_3 is needed for analyses of potential accident scenarios involving corroded metal or SNF. Specifically, kinetic rate laws for the UH_3–O_2 and UH_3–H_2O reactions are of interest.

Characterization of metallic uranium fuel plates used in the Zero Power Physics Reactor (ZPPR) that had corroded during extended vault storage was undertaken in 1996 to obtain needed information on the formation of UH_3 during storage. The plates are U metal coupons clad in stainless steel jackets with porous metal endplugs. The presence of the cladding and the access of the ambient gas environment, which included water vapor, to the metal via the endplugs led to severe localized corrosion. Examination of the loose corrosion products associated with the plates revealed that they contained high levels of UH_3, 50–85% in some cases [10,18]. These figures did not include adherent oxides remaining on the plates.

Because of their high UH_3 contents, these corrosion products represent a good test material for measuring the kinetics of UH_3 formed by corrosion of uranium metal. This paper presents the results of TGA oxidation testing of the corrosion products undertaken to quantify their reactivity in terms of ignition temperatures, oxidation rates, and hydride fractions. TGA testing was performed with three O_2 concentrations – 4%, 9%, and 20% – to assess the effect of O_2 concentration on ignition temperatures and oxidation rates. The results of specific surface area measurements of the corrosion products, performed using a technique based on the Brunauer, Emmett, and Teller (BET) theory of gas adsorption, are also presented, along with X-ray diffraction (XRD) analyses of the products performed before and after TGA testing.

2. Experimental procedures

2.1. Corrosion product sampling

Six corroded U metal ZPPR fuel plates were selected to obtain products for BET, TGA, and XRD analysis. The corrosion products are mixtures of UO_2 and UH_3; detailed descriptions of the ZPPR plates and their corrosion products may be found in Refs. [18,10]. Table 1 lists the plates, their degrees of corrosion, and the testing performed on their corrosion products. The degree of corrosion was assessed both by a visual ranking of the relative degree of cladding bulging and by the amount of loose corrosion product collected. The previous characterization work had identified exterior bulging of the cladding as an indicator of severity of localized corrosion [18]. The plates were de-clad in a pass-through Ar glovebox (O_2 content less than 0.15%; H_2O not analyzed), and the loose corrosion products were separated from the plates with a horse-hair brush and collected. The brushing left an adherent oxide layer on the metal plates. The moderate and severely corroded plates had significantly larger quantities of loose corrosion products than the lightly corroded plates. There was little difference, however, between the amount of loose products collected from moderately corroded plates and that from severely corroded plates, contrary to indications from exterior appearance. The total metal mass for each plate was approximately 220 g. After collection, the product samples from the three plates were transferred into a purified Ar glovebox (O_2 and H_2O contents less than 10 ppm each) for storage, preparation of BET and XRD samples, and TGA testing.

Table 1
Corrosion extent and analysis techniques for ZPPR plates

Plate ID	Relative corrosion extent	Mass of loose corrosion product (g)	BET	TGA	XRD
2249	Light	1.42	X	X	X
2652	Moderate	4.35	X	X	X
2962	Severe	3.39	X		
3401	Moderate	4.03	X	X	
3411	Severe	2.40	X		
3930	Light	1.67	X		

2.2. Specific surface area measurement

Specific surface area measurements were performed on corrosion product samples from all six plates using a Quantachrome Quantasorb gas sorption analyzer and standard BET techniques [19] with Kr gas as the adsorbate, He gas as the carrier, and N_2 gas for calibration. Adsorption was carried out at liquid N_2 temperature (77 K); three consecutive measurements were made on each sample. The test matrix and results are shown in Table 2.

2.3. Oxidation testing

Oxidation testing of corrosion products from plates 2249, 2652, and 3401 was carried out using a modified Shimadzu TGA-51H TGA in a purified Ar glovebox. Modifications to the instrument were made to enable control of gas composition, flow rate, and pressure in the sample chamber and to allow the use of a computer located outside the glovebox for TGA control and data acquisition. The TGA balance has a stated resolution of 1 μg. The accuracy of the balance was checked against NIST-traceable weight standards of 5, 20, and 50 mg. The TGA reading was accurate to greater than 2% for all weights. The accuracy of the TGA control thermocouple was checked against a second, calibrated thermocouple and found to agree within 5°C.

The TGA test matrix and results are shown in Table 3. Most tests were performed under 'isothermal' conditions at temperatures from 50°C to 250°C. For isothermal tests the TGA furnace was programmed to ramp to the test temperature and then maintain that temperature. Ramp rates varied from 5°C/min to 30°C/min; the test chamber was purged with ultra-high purity Ar during the heat-up period. When the test temperature was reached and stabilized, an Ar–30%O_2 reacting gas was admitted into the chamber by opening a solenoid valve in its supply line. The net O_2 concentration in the chamber was controlled by varying the flow rates of the reacting gas and the pure Ar purge gas. The two gas streams mixed just prior to entering chamber. A few tests were performed in which the gas flows were not set properly prior to testing, and hence the O_2 concentrations and flows were not as planned (ZPPR 17, 19, and 30). The actual O_2 concentrations and flows are recorded in Table 3.

The weight of the sample was recorded for the duration of the test. Ignition in an isothermal test was indicated by a rapid increase in sample weight and a simultaneous increase in furnace thermocouple reading, the latter due to heat evolved by oxidation.

Several tests performed were of the 'burning curve' type. The burning curve test has been commonly used in the past to measure ignition temperatures. For this type of test the furnace temperature was programmed to increase at a constant rate (15°C/min) until the desired temperature was reached. Both reacting and purge gas flows were on during the entire heat-up period. Ignition was indicated by either a rapid increase in sample weight and commensurate increase in furnace thermocouple reading, or a rapid increase in sample thermocouple reading and commensurate increase in furnace thermocouple reading. The latter was observed for tests in which a sample thermocouple was placed in contact with the sample. For these tests the weight of the sample could not be measured.

No specific measures were taken to insure that individual TGA samples were representative of the overall corrosion product from a given plate. The 100–300 mg samples were simply scooped out of the polyethylene bottle in which the corrosion products from that plate were stored and placed into a platinum sample pan for testing. The samples tested were a mixture of UO_2 (and/or U_3O_7) and UH_3 (see Section 3.3). The oxide generally took the form of gray flakes or powder, while the hydride was a black powder [10]. All tests were performed at a nominal total pressure of 70 kPa. A total gas flow of 3.3 cm^3/s was used for nearly all tests, with exceptions as described above.

2.4. X-ray diffraction

XRD was used for identification of phases present in the loose corrosion products of plates 2249 and 2652, and for determining the stoichiometry of oxides formed during TGA oxidation of the loose corrosion products. All samples were crushed to a fine powder in a high-purity Ar glovebox and then loaded into a sealed environmental chamber. Diffraction was performed on a

Table 2
BET test matrix and results

Plate ID	Sample weight (g)	Surface area (m^2)	Specific surface area (m^2/g)
2249	1.09	0.54–0.57	0.50–0.52
2652	0.71	0.54–0.57	0.75–0.80
2962	2.11	2.00–2.20	0.95–1.04
3401	3.07	2.25–2.40	0.73–0.78
3411	2.30	1.69–1.75	0.74–0.76
3930	1.56	1.18–1.21	0.76–0.77

Table 3
TGA testing matrix and results

Test ID	Source plate	Specific area (m^2/g)	Weight (mg)	Hydride surface (cm^2)	Test type	Temperature (°C)	Test time (min)	Environment	Ignition (Y/N)	Kinetics	Burning rate (mg/s)	Low-Temp. oxidation rate ($mg/cm^2/s$)	Hydride fraction (wt%)
ZPPR 33	2652	0.8	120.5	280	Isothermal	50	967	Ar–4%O_2, 200 ml/min	No	Decreasing rate	N/A	3.6E-09	N/A
ZPPR 39	2652	0.8	166.5	450 [a]	Isothermal	75	580	Ar–4%O_2, 200 ml/min	No	Linear	N/A	1.8E-08	N/A
ZPPR 29	2652	0.8	122.6	340 [a]	Isothermal	100	580	Ar–4%O_2, 200 ml/min	No	Decreasing rate	N/A	7.4E-08	N/A
ZPPR 28	2652	0.8	121.6	330 [a]	Isothermal	125	233	Ar–4%O_2, 200 ml/min	No	Decreasing rate	N/A	3.9E-07	N/A
ZPPR 36	2652	0.8	169.7	N/A	Isothermal	150	58	Ar–4%O_2, 200 ml/min	Yes	Linear, then Decr.	8.9E-03	N/A	N/A
ZPPR 24	2652	0.8	178.0	N/A	Isothermal	150	98	Ar–4%O_2, 200 ml/min	Yes	Linear, then Decr.	9.2E-03	N/A	N/A
ZPPR 33A	2652	0.8	120.5	280	Isothermal	200	47	Ar–4%O_2, 200 ml/min	Yes	Linear, then Decr.	1.2E-02	N/A	29
ZPPR 25	2652	0.8	118.1	290	Isothermal	200	90	Ar–4%O_2, 200 ml/min	Yes	Linear, then Decr.	9.9E-03	N/A	31
ZPPR 31	2652	0.8	114.5	300	Isothermal	250	90	Ar–4%O_2, 200 ml/min	Yes	Linear, then Decr.	1.1E-02	N/A	33
ZPPR 26	2652	0.8	131.7	310	Burning Curve	15°C/min	25	Ar–4%O_2, 200 ml/min	Yes	$T_{ig} = 145$°C	1.2E-02	N/A	29
ZPPR 27	2652	0.8	134.1	N/A	Burning Curve	15°C/min	12	Ar–4%O_2, 200 ml/min	Yes	$T_{ig} = 143$°C	$T_{max} = 201$°C	N/A	N/A
ZPPR 04	3401	0.8	179.7	676	Isothermal	100	26	Ar–9%O_2, 200 ml/min	No	Decreasing rate	N/A	1.8E-07	47
ZPPR 05	3401	0.8	151.1	653	Isothermal	125	6	Ar–9%O_2, 200 ml/min	Yes	Linear	6.1E-02	N/A	54
ZPPR 01	3401	0.8	199.9	768	Isothermal	150	7	Ar–9%O_2, 200 ml/min	Yes	Linear	6.5E-02	N/A	48
ZPPR 02A	3401	0.8	110.0	431	Isothermal	150	5	Ar–9%O_2, 200 ml/min	Yes	Linear	7.3E-02	N/A	49
ZPPR 04A	3401	0.8	179.7	676	Isothermal	150	8	Ar–9%O_2, 200 ml/min	Yes	Linear	5.1E-02	N/A	47
ZPPR 06	3401	0.8	194.4	840	Isothermal	200	8	Ar–9%O_2, 200 ml/min	Yes	Linear	5.7E-02	N/A	54
ZPPR 07	3401	0.8	117.6	480	Burning Curve	15°C/min	13	Ar–9%O_2, 200 ml/min	Yes	$T_{ig} = 142$°C	5.9E-02	N/A	51

Table 3 (*Continued*)

Test ID	Source plate	Specific area (m^2/g)	Weight (mg)	Hydride surface (cm^2)	Test type	Temperature (°C)	Test time (min)	Environment	Ignition (Y/N)	Kinetics	Burning rate (mg/s)	Low-Temp. oxidation rate ($mg/cm^2/s$)	Hydride fraction (wt%)
ZPPR 20	2652	0.8	203.7	570	Isothermal	125	4	Ar–20%O_2, 200 ml/min	Yes	Linear	1.3E-01	N/A	35
ZPPR 23	2652	0.8	181.0	540	Isothermal	125	4	Ar–20%O_2, 200 ml/min	Yes	Linear	1.1E-01	N/A	37
ZPPR 17	2652	0.8	201.7	570	Isothermal	150	5	Ar–27%O_2, 150 ml/min	Yes	Linear	1.2E-01	N/A	35
ZPPR 18	2652	0.8	215.2	600	Isothermal	150	5	Ar–20%O_2, 200 ml/min	Yes	Linear	1.2E-01	N/A	35
ZPPR 19	2652	0.8	130.1	340	Isothermal	200	4	Ar–27%O_2, 150 ml/min	Yes	Linear	1.3E-01	N/A	33
ZPPR 30	2652	0.8	105.0	250	Isothermal	250	5	Ar–21%O_2, 40 ml/min	Yes	Linear	2.5E-02	N/A	30
ZPPR 21	2652	0.8	253.0	790	Burning Curve	15°C/min	12	Ar–20%O_2, 200 ml/min	Yes	$T_{ig} = 134$°C	1.1E-01	N/A	39
ZPPR 22	2652	0.8	193.0	N/A	Burning Curve	15°C/min	12	Ar–20%O_2, 200 ml/min	Yes	$T_{ig} = 137$°C	$T_{max} = 487$°C	N/A	N/A
ZPPR 15	3401	0.8	122.6	334	Isothermal	60	600	Ar–20%O_2, 200 ml/min	No	Decreasing rate	N/A	8.5E-09	52
ZPPR 10	3401	0.8	121.6	902	Isothermal	100	26	Ar–20%O_2, 200 ml/min	No	Decreasing rate	N/A	1.4E-07	61
ZPPR 13	3401	0.8	169.7	591	Isothermal	100	300	Ar–20%O_2, 200 ml/min	No	Decreasing rate	N/A	7.1E-08	52
ZPPR 12	3401	0.8	178.0	376	Isothermal	125	90	Ar–20%O_2, 200 ml/min	No	Decreasing rate	N/A	4.0E-07	51
ZPPR 08	3401	0.8	120.5	226	Isothermal	150	2.5	Ar–20%O_2, 200 ml/min	Yes	Linear	1.0E-01	N/A	54
ZPPR 10A	3401	0.8	118.1	902	Isothermal	150	5	Ar–20%O_2, 200 ml/min	Yes	Linear	9.6E-02	N/A	61
ZPPR 11A	3401	0.8	114.5	386	Isothermal	150	4	Ar–20%O_2, 200 ml/min	Yes	Linear	9.5E-02	N/A	55
ZPPR 12A	3401	0.8		376	Isothermal	150	4	Ar–20%O_2, 200 ml/min	Yes	Linear	1.4E-01	N/A	51
ZPPR 16	3401	0.8	131.7	78	Isothermal	150	220	Ar–20%O_2, 200 ml/min	No	Decreasing rate	N/A	7.1E-07	53

Table 3 (*Continued*)

Test ID	Source plate	Specific area (m^2/g)	Weight (mg)	Hydride surface (cm^2)	Test type	Temperature (°C)	Test time (min)	Environment	Ignition (Y/N)	Kinetics	Burning rate (mg/s)	Low-Temp. oxidation rate ($mg/cm^2/s$)	Hydride fraction (wt%)
ZPPR 09	3401	0.8	134.1	269	Isothermal	200	2.5	Ar–20%O_2, 200 ml/min	Yes	Linear	1.1E-01	N/A	57
ZPPR 13A	3401	0.8		591	Isothermal	200	4	Ar–20%O_2, 200 ml/min	Yes	Linear	1.1E-01	N/A	52
ZPPR 14A	3401	0.8	141.1	452	Isothermal	200	4	Ar–20%O_2, 200 ml/min	Yes	Linear	1.2E-01	N/A	58
ZPPR 15A	3401	0.8	101.5	334	Isothermal	250	3	Ar–20%O_2, 200 ml/min	Yes	Linear	1.1E-01	N/A	52
ZPPR 35	2249	0.5	141.1	706 [b]	Isothermal	150	580	Ar–20%O_2, 200 ml/min	No	Decreasing rate	N/A	4.7E-09	N/A
ZPPR 34	2249	0.5	205.0	1030 [b]	Isothermal	200	108	Ar–20%O_2, 200 ml/min	No	Decreasing rate	N/A	8.8E-07	N/A
ZPPR 32	2249	0.5	101.5	N/A	Burning Curve	15°C/min	25	Ar–20%O_2, 200 ml/min	No	N/A	N/A	N/A	N/A

[a] Average hydride fraction for the plate used to calculate hydride surface area.

[b] For these tests total surface area rather than hydride surface area was used to calculate oxidation rates.

Scintag X1 powder diffractometer using Cu K-alpha radiation. The scan range was from 20° to 100° 2θ with a scan rate of 0.75 degrees per minute. Standardless quantitative analysis of the diffraction patterns from the corrosion product samples was performed using Sietronics XRD phase analysis software to estimate the fraction of hydride present in the samples for comparison with the TGA results.

3. Results

3.1. Specific surface areas

Table 2 presents specific surface areas measured for the loose corrosion products collected from the six plates. Given the wide range in extent of corrosion among the six plates tested, the specific surface areas measured were remarkably consistent. Values ranged from a low of 0.51 m^2/g for plate 2249 to a high of 1.00 m^2/g for plate 2962. The specific surface areas of four out of six plates were between 0.74 and 0.80 m^2/g.

3.2. TGA results

3.2.1. Data analysis

Table 3 presents data obtained in TGA oxidation testing of corrosion products from plates 2249, 2652, and 3401. The data for isothermal tests were analyzed by plotting the weight gain of the sample as a function of test time. The initiation of reacting gas flow was taken to be the start of the test. For nearly all tests, the weight gain of the sample was ascribed to reaction of UH_3 with O_2 to form uranium oxide. This oxide was assumed to be U_3O_8 for tests in which burning occurred. XRD analysis of the reacted material, described in Section 3.5, supports this assumption.

For tests in which ignition occurred, the weight gain as a function of time was approximately linear, as shown in Fig. 1. The slope was taken to be the burning rate of the sample, i.e. the rate of oxidation above the ignition temperature. Burning rates are reported in Table 3. The burning rates are given in units of mg/s rather than mg/cm^2/s because the observed rates of weight gain were independent of sample size and hence surface area. Normalizing the burning rates by surface area considerably increased the scatter in the data, which was very consistent without normalization.

Oxidation of samples for which ignition did not occur was characterized by a decreasing rate of weight gain with increasing test time. Attempts to fit the low-temperature oxidation data with parabolic or paralinear rate kinetics for the entire test duration were not successful; no single rate law provided a good fit to all tests. In order to make comparisons between tests at different

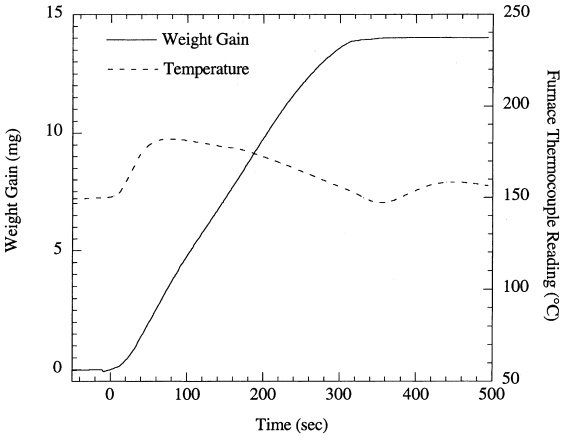

Fig. 1. Plot of weight gain and furnace temperature for ignition and burning of plate 3401 corrosion product in Ar–9%O_2 (ZPPR 4A).

temperatures, best linear fits were made to the weight gain versus time curves. The fits were made to all of the data after the initial parabolic weight gain. Because the rate of oxidation did not change significantly over the course of a test, the error introduced by the somewhat arbitrary fit was small, especially relative to the overall scatter in the rates as a function of temperature.

The hydride contents of the oxide–hydride samples were calculated from the total weight gain observed after completion of burning, which was clearly indicated by the sample weight becoming stable (Fig. 1). The calculation was performed by computing the weight of hydride needed to produce the weight gain observed according to the stoichiometry of reaction (2) and then dividing this weight by the total sample weight to obtain the hydride fraction. The weight gain due to conversion of UO_2 to U_3O_7 or U_3O_8 was neglected due to the limited maximum sample temperature (~500°C), short test duration, and the low percentage weight gains for these reactions relative to UH_3 oxidation. Further basis for this assumption is presented in Section 4.3.

The computed hydride fraction was further used to compute the original hydride surface area in the sample, which was taken as the product of the specific surface area, the original sample mass, and the hydride fraction. For the purposes of calculation, the hydride component of the sample was assumed to have the same specific area as the oxide component. The validity of this assumption is supported by the similarity of specific areas for corrosion products with differing hydride contents.

Most samples that were tested at lower temperatures and which did not ignite were subsequently tested again at a higher-temperature in order to completely oxidize the sample and compute a hydride fraction. The second, high-temperature test for a given sample is denoted by the suffix A. The results from these tests are also

included in Table 3, as the small amount of oxidation incurred in the first test was not believed to alter the burning kinetics observed in the second, high temperature test. The consistency of results from the A tests with other tests at same conditions supports this assumption. For samples which were not completely oxidized in a second test, the average hydride content of other samples from the same plate was used to compute the hydride surface area. The hydride surface area (computed or measured) was used to normalize oxidation rates for all low-temperature tests.

3.2.2. Plate-to-plate variations

Table 4 summarizes the TGA reactivity characteristics – ignition temperature, burning rate, and hydride content – of the corrosion products from plates 2249, 2652, and 3401. Plates 2652 and 3401 were both moderately corroded, while plate 2249 showed very little corrosion. The ignition temperatures and burning rates of products from the two moderately corroded plates were very similar. The ignition temperature of the one sample from plate 3401 tested in a burning curve mode in Ar–9%O_2 was 142°C. The two ignition temperatures measured in a burning curve mode for samples from plate 2652 were 134 and 137°C. These tests were performed in Ar–20%O_2. For isothermal tests in Ar–20%O_2, ignition was observed occasionally at 125°C and consistently at 150°C for samples from both plates. The burning rates in Ar–20%O_2 were also very consistent. The rates for samples from plate 3401 varied from 0.095 to 0.141 mg/s; the rates for plate 2652 varied from 0.112 to 0.128 mg/s.

The hydride content measured by TGA was observed to differ for the two moderately corroded plates. The hydride fractions for plate 3401 samples varied from 47 to 61 wt%, while the hydride fractions for plate 2652 samples varied from 29 to 39 wt%. The properties of plate 2249, which did not show significant localized corrosion, were very different from the other two plates. Ignition was not observed in any of the samples tested from this plate, even at temperatures of up to 500°C (in the one burning curve test). The rate of weight gain in an isothermal test at 150°C was approximately 4×10^{-6} mg/s, several orders of magnitude less than the burning rates observed for the two other plates at the same temperature.

3.2.3. Burning kinetics

The results of the tests performed in varying O_2 concentrations (4%, 9%, and 20%) showed that burning was not as vigorous in Ar–4%O_2 as it was in Ar–9%O_2 and Ar–20%O_2. As described in Section 3.2.1, ignition and burning was indicated by a rapid rate of weight gain and a corresponding increase in furnace control thermocouple temperature. In Ar–9%O_2 and Ar–20%O_2, a high rate of weight gain was maintained until oxidation was nearly complete, and the furnace temperature increase was substantial. Fig. 1 shows a typical plot of weight gain and furnace temperature during burning in Ar–9%O_2 at 150°C. In contrast, the shapes of the weight gain versus time curves for burning in Ar–4%O_2 were characterized by an initially high, linear rate of weight gain which underwent a marked slowing after approximately three-quarters of the sample was consumed. In addition, the increase in furnace control thermocouple reading was smaller. Fig. 2 is a plot showing this behavior.

There was little, if any, effect of O_2 concentration on ignition temperature. In Ar–20%O_2, the ignition temperatures measured in two burning curves tests (ZPPR 21 and 22) were 134°C and 137°C. The burning curve ignition temperature in one test in Ar–9%O_2 (ZPPR 07) was 142°C, and the burning curve ignition temperatures measured in two tests in Ar–4%O_2 (ZPPR 26 and 27) were 143°C and 145°C.

The rates of oxidation above the ignition temperature were found to be strongly dependent on O_2 concentration, contrary to the lack of an effect observed for the ignition temperature. A strong correlation was found to exist between the burning rate and the net rate of O_2 flow in the sample chamber. The net rate of O_2 flow was computed as the total flow rate multiplied by the O_2 concentration. Fig. 3 is a plot of burning rate in mg/s versus net O_2 flow rate in cm^3/s showing this trend. Data from plates 2652 and 3401 at a variety of O_2 concentrations are plotted.

Two burning curve tests were performed to measure the maximum sample temperatures achieved during burning in Ar–20%O_2 and Ar–4%O_2. Fig. 4 shows a plot of furnace and sample thermocouple temperatures as a function of time for a burning curve test in Ar–20%O_2 (ZPPR 22). At the ignition temperature, the sample thermocouple reading dramatically increased to a maximum value of 487°C and then gradually de-

Table 4
Ar–20%O_2 reactivity characteristics summary

Plate ID	Ignition temperature (°C)	Burning rate (mg/s)	Hydride (%)
3401	BC [a]: 142 (9% O_2) isothermal: $\geqslant$125	0.10–0.14 average: 0.11	47–61 (TGA)
2652	BC: 134–137 isothermal: $\geqslant$125	0.11–0.13 average: 0.12	29–39 (TGA) 47 (XRD)
2249	ignition not observed	no burning rate at 150°C: 4×10^{-6}	3 (XRD)

[a] Burning curve.

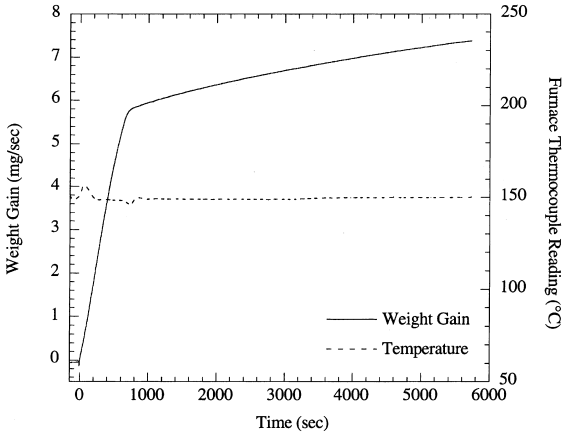

Fig. 2. Plot of weight gain and furnace temperature for ignition and burning of plate 2652 corrosion product in Ar–4%O_2 (ZPPR 24).

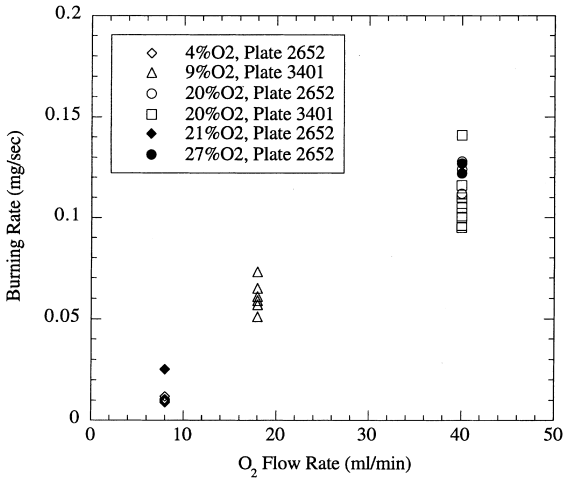

Fig. 3. Variation of burning rate with net oxygen flow rate.

creased as the sample was consumed. As shown in Fig. 5, the maximum burning temperature observed for a similar test in Ar–4%O_2 (ZPPR 27) was much lower, only 201°C. The difference is attributed to the considerably slower rate of burning in Ar–4%O_2.

3.2.4. Low-temperature oxidation kinetics

There appeared to be little effect of oxygen concentration on oxidation kinetics below the ignition temperature. Fig. 6 is an Arrhenius plot of the low temperature oxidation rates versus temperature. All data fall roughly into a straight line, with a large scatter at 100°C (where several tests were performed) clearly evident. The data obtained in 4% O_2 fit reasonably well within the scatter of the higher O_2 concentration data. Fig. 6 also shows a linear regression fit to the data. The rate equations obtained are

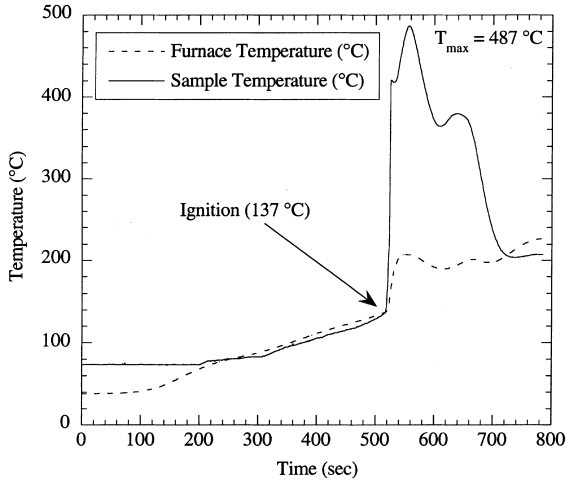

Fig. 4. Sample and furnace thermocouple readings for burning of plate 2652 corrosion product in Ar–20%O_2 (ZPPR 22).

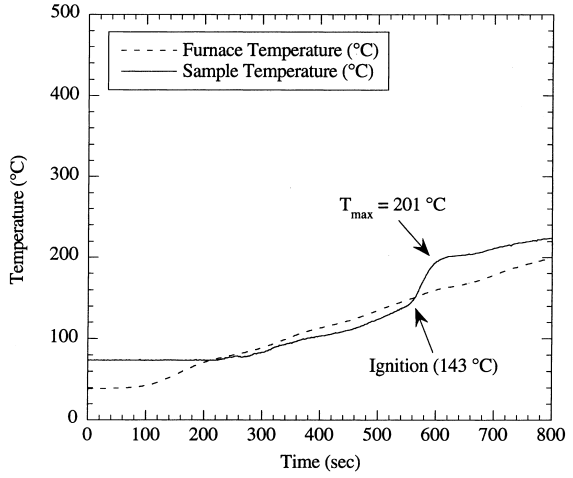

Fig. 5. Sample and furnace thermocouple readings for burning of plate 2652 corrosion product in Ar–4%O_2 (ZPPR 27).

$$k = 67\exp(-Q/RT)\mathrm{mg/cm^2/s}, \tag{3}$$

$$Q = 63 \pm 4\ \mathrm{kJ/mol} \tag{4}$$

where k is the linear rate constant and Q is the activation energy. The linear rate constant applies to a rate equation of the form $\Delta W = kt$, where ΔW is the weight gain per unit surface area and t is time. The relation is valid over the temperature range of 50–150°C.

3.3. X-ray diffraction analysis

Standardless quantitative analysis of XRD patterns from corrosion product samples of plates 2652 and 2249 provided a second means of measuring UH_3 contents.

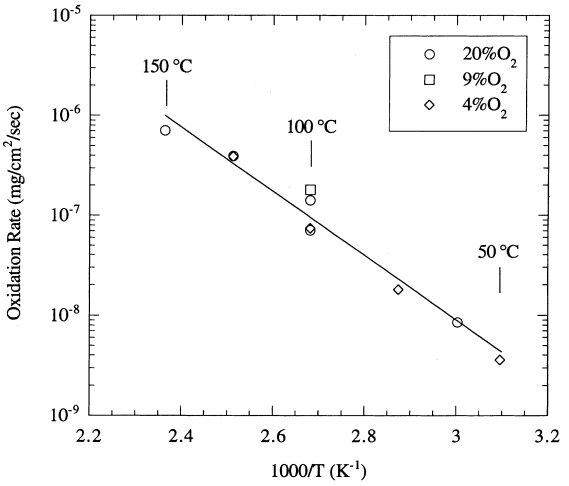

Fig. 6. Arrhenius plot of best linear fit oxidation rates versus reciprocal temperature.

Using this technique, the sample from plate 2652 was determined to be comprised of approximately 47 wt% UH_3 and 53 wt% UO_2. The hydride fraction for plate 2652 determined by TGA analysis varied from 29 to 39 wt%.

XRD analysis of TGA samples after burning in environments of Ar–4%O_2, Ar–9%O_2, and Ar–20%O_2 showed only oxide phases. The peaks observed in these samples were very broad (this was also true for non-reacted samples). Because of the peak width and the similarity of lattice parameters, it was not possible to differentiate between UO_2 and U_3O_7 or U_3O_8 and UO_3 with any reasonable certainty. Based on literature information [1] and the results of TGA tests on plate 2249, the oxide present in non-reacted samples is believed to be UO_2. For samples tested in Ar–9%O_2 and Ar–20%O_2 (ZPPR 04 and 13) both UO_2/U_3O_7 and U_3O_8/UO_3 were observed. The higher oxides are believed to result from the reaction of UH_3 with O_2. The lower oxides could either be UO_2 present in the sample prior to testing, U_3O_7 formed by oxidation of UO_2 during testing, or a combination of the two. Oxide present in the loose corrosion products from ZPPR plates has a distinct flake-like morphology [18] which did not appear to change as a result of TGA testing. The lack of change suggests that the extent of UO_2 oxidation in these samples is small. Only UO_2/U_3O_7 peaks were observed in the sample tested in Ar–4%O_2 (ZPPR 25). The lower oxygen concentration in the reacting gas appears to have prevented the formation of higher oxides during oxidation of UH_3.

The sample from plate 2249 was found by XRD to have only 3 wt% UH_3 (remainder UO_2/U_3O_7) a result which is consistent with the lack of reactivity observed in the TGA tests. Due to the peak width and similarity of the UO_2 and U_3O_7 lattice parameters mentioned above, it was not possible to verify using XRD that the weight gains observed in these tests (ZPPR 34 and 35) were in fact a result of UO_2 oxidation to U_3O_7.

Despite the variety of oxide phases observed in the reacted TGA samples, for the purposes of calculating UH_3 contents based on TGA weight gain only U_3O_8 was assumed to be formed. As stated above, the oxides with peaks which could correspond to either U_3O_8 or UO_3 were believed to be formed during TGA oxidation in 9% and 20% O_2. Of the two higher oxides, U_3O_8 was chosen for the calculations because it has been cited in the literature [12,14] as the reaction product of UH_3 with air. The error introduced by the use of U_3O_8 for UH_3 calculations for tests in Ar–4%O_2 appears to be small since the calculated UH_3 fractions for tests in Ar–4%O_2 lie within the range of values computed for the samples from the same plate (2652) tested in Ar–20%O_2.

4. Discussion

4.1. Specific surface areas

The specific surface areas measured for the loose corrosion products (mixtures of oxide and hydride) fall within the range of values reported for pure UH_3. Longhurst [17] reported specific areas between 0.3 and 0.6 m^2/g, Stakebake [16] reported 2.8 m^2/g, and Alire [20] reported 0.8–1.1 m^2/g. All were prepared by hydriding U metal. The specific areas of uranium oxide powders vary greatly depending on the means of preparation [21]. Oxides formed as corrosion products are not typically analyzed for specific surface area, so a direct comparison with the current data cannot be made.

4.2. Ignition temperatures and burning rates

The behavior of the hydride-bearing ZPPR corrosion products observed in this series of tests was very comparable to observed by Longhurst [17] in his tests on pure UH_3. The ignition temperatures in this series of tests, 134–145°C, bracket the 140°C value reported by Longhurst. In Longhurst's case, however, the heat of burning was sufficient to melt the Pt sample pan, indicating that the burning temperature exceeded 1772°C. Burning temperatures of ZPPR corrosion products in the present study did not exceed 500°C. The source of this difference is unknown. In the study by Stakebake [16], ignition was observed as low as 0°C, as evidenced by the relatively rapid total reaction of the hydride powder (3 min) and the 75°C temperature excursion of the recording thermocouple at this test temperature. This lower ignition temperature may be a result of the greater specific surface area of the powder tested by

Stakebake (2.8 m^2/g) compared to that of Longhurst (0.3–0.6 m^2/g) and the present study (0.5–1.0 m^2/g).

It must be noted that ignition temperatures measured in TGA testing do not necessarily reflect the behavior of the corrosion product under actual handling conditions. The samples in TGA testing are quiescent, while handling introduces energy to the samples via mechanical agitation or static discharge. Mechanical agitation may lead to fracture of passivating oxide films present on hydride particles, thereby exposing the reactive hydride to oxygen. Ignition of ZPPR fuel corrosion product powders has occurred during handling at room temperature [18].

The strong dependence of burning rate on net O_2 flow rate over a range of flows, O_2 concentrations, test temperatures, sample sizes, and source plates indicates that, for these TGA tests, the burning rate of ZPPR fuel corrosion products was limited by convective oxygen transport in the gas phase, rather than by any intrinsic material property. Additional support for this hypothesis is provided by the fact that the rate of sample mass gain was approximately the same as the O_2 mass flow rate past the sample pan. For 20% O_2 at 3.3 cm^3/s at a test temperature of 150°C, multiplication of the net O_2 flow rate (0.7 cm^3/s) by the density of O_2 at 150°C (0.92 mg/cm^3) yields an O_2 mass flow rate of approximately 0.6 mg/sec. The sample chamber is a 25 mm cylinder through which the reacting gas flows. The circular sample pan is located in the center of the sample chamber (concentric) and has a 10 mm diameter. The ratio of the area of the sample pan to the chamber area is 1/6; therefore, to a first approximation the flow which impinges on the sample pan is 1/6 of the total flow, or 0.1 mg/s. This value is in agreement with the observed rate of mass gain for burning in Ar–20%O_2. Similar agreement is seen for burning rates in 4% O_2 and 9% O_2.

4.3. Hydride concentrations

The hydride contents observed for corrosion products from the two moderately corroded plates are fairly high for uranium metal corrosion products. Typical hydride contents reported for reaction products of uranium metal with water vapor are less than 20% [4,8,22]. It must be noted, however, that the hydride contents measured in the current tests only apply to the loose corrosion product. The hydride content for the corrosion product from an entire plate should be lower, as the tightly adherent product remaining on the plates is believed to be oxide. Relatively high hydride contents were also observed in the previous characterization work [10]. A potential mechanism cited for the formation of high UH_3 was preferential permeation of H_2O through an elastomer seal used on the canisters in which the clad plates were stored. The reaction would then be between U and H_2O only, with the corrosion crevices acting to trap H_2 formed in the reaction, allowing it to react with metal to form hydride.

Both TGA and XRD results indicate that there is very little hydride present in the loose corrosion product from plate 2249. This observation is consistent with XRD data produced from a sample from another plate, 4414, which was also characterized as showing little localized corrosion [10]. No UH_3 peaks were identified in this sample, contrary to the strong hydride peaks observed in corrosion product samples from more badly corroded plates.

The small weight gain that was observed in the isothermal tests of plate 2249 corrosion products at 150°C and 200°C may be a result of oxidation of UH_3 or UO_2. UO_2 powders will measurably oxidize to U_3O_7 between 100°C and 250°C [23]. It is not possible to conclusively differentiate between these two reactions, but the weight gains observed in the isothermal tests are in good agreement with weight gains calculated using the parabolic rate constant given in Ref. [23]. These rates are orders of magnitude less than UH_3 burning rates or non-burning oxidation rates observed at the same temperatures for samples from plates 2652 and 3401, hence the assumption that the weight gain for tests on samples which contained appreciable UH_3 was only due to UH_3 oxidation is valid.

The reason for the discrepancy between the hydride contents measured by TGA and those calculated from the XRD patterns is unknown. Neither technique is a highly accurate way of assessing UH_3 contents. The XRD analysis is standardless and complicted by the large peak width. The TGA technique relies on an assumption that the reaction product of UH_3 and O_2 is U_3O_8. The accuracy of both measurement techniques are believed to be 10% at best. While it is also possible that the XRD sample was intrinsically different than the TGA samples, this is unlikely. The results from the TGA samples were fairly consistent, and the XRD sample was collected in the same manner as the TGA samples.

4.4. Low-temperature oxidation kinetics

The data obtained in this study of UH_3 oxidation are compared with uranium metal oxidation data [1] in Fig. 7. The comparison is made on the basis of the weight of uranium or uranium hydride reacted rather than weight gain, since the weight gains associated with the reaction of an equivalent number of U atoms are different for oxidation of U metal and U hydride. It is interesting that the slope of the regression fit is very similar to the slope for uranium metal. A similar activation energy suggests that the rate-determining mechanism of oxidation is similar. In both cases the mechanism is expected to be diffusion of oxygen (as an O^{2-} ion) through a uranium oxide film, as both reactions have uranium oxide products. The magnitude of the

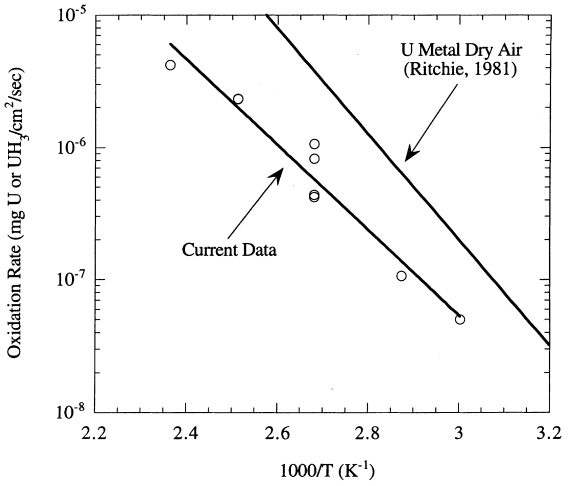

Fig. 7. Comparison of current data with U metal oxidation rates from Ritchie [1].

rates are comparable, although the hydride data are a factor of 5–10 less than the oxide data. This difference is likely within the scatter of the U metal data reviewed by Ritchie [1].

There was little observed effect of O_2 concentration on low-temperature oxidation rates of ZPPR corrosion product powders. Oxidation theory does predict an effect of O_2 partial pressure on U metal oxidation rates [2], but it is small (the reported dependence is proportional to $p_{O_2}^{1/5}$). Assuming that UH_3 oxidizes by the same mechanism as U metal, this dependence would be hidden by the intrinsic scatter of the corrosion product oxidation data.

5. Conclusions

The oxidation behavior of uranium metal corrosion products from ZPPR fuel plates was studied using TGA, XRD, and BET gas sorption analysis. The following conclusions were reached.

1. The specific surface areas of the loose corrosion products varied from 0.51 to 1.00 m^2/g.
2. Ignition of samples from the two moderately corroded plates was observed between 125°C and 150°C. There was little variation in observed ignition temperature between the two plates or with variation in oxygen concentration in the reacting gas.
3. The rate of oxidation above the ignition temperature was dependent only on the net flow rate of oxygen in the reacting gas for the range of flows and oxygen concentrations investigated.
4. Oxidation rates below the ignition temperature decreased with increasing test time. These rates were apparently independent of oxygen concentration between 4% and 20% oxygen. Best linear fit approximations to the data were used to determine an activation energy.
5. There was a difference in hydride content in the loose corrosion product for the two moderately corroded plates, 47–61 wt% versus 29–39 wt%.
6. The corrosion products from a plate which showed relatively little signs of corrosion were not reactive and contained little uranium hydride.

Acknowledgements

The authors wish to acknowledge E.A. Beverly, R.W. Bratt, and R.J. Briggs for assistance in obtaining corrosion product samples. This work was supported through funding by the US Department of Energy, Reactor Systems, Development and Technology, under contract W-31-109-Eng-38, and by the US Department of Energy National Spent Nuclear Fuel Program.

References

[1] A.G. Ritchie, J. Nucl. Mater. 102 (1981) 170.
[2] C.A. Colmenares, Prog. Solid State Chem. 15 (1984) 257.
[3] C.A. Colmenares, Prog. Solid State Chem. 9 (1975) 139.
[4] M.M. Baker, L.N. Less, S. Orman, Trans. Faraday Soc. 62 (1966) 2513.
[5] L.J. Weirick, The oxidation of uranium in low partial pressures of oxygen and water vapor at 100°C, Sandia National Laboratory Report SAND83-0618, 1984.
[6] A.G. Ritchie, J. Nucl. Mater. 120 (1984) 143.
[7] C.A. Colmenares, R. Howell, T. McCreary, Oxidation of uranium studied by gravimetric and positron-annihilation techniques, Lawrence Livermore National Laboratory Report UCRL-85549, 1981.
[8] T. Kondo, F.H. Beck, M.G. Fontana, Corrosion 30 (1974) 330.
[9] V.H. Troutner, Mechanisms and kinetics of uranium corrosion and uranium core fuel element ruptures in water and steam, Hanford Atomic Products Operation Report HW-67370, 1960.
[10] T.C. Totemeier, R.G. Pahl, S.L. Hayes, S.M. Frank, J. Nucl. Mater. 256 (1998) 87.
[11] S.C. Marschman, T.D. Pyecha, J. Abrefah, Metallographic examination of damaged N reactor spent nuclear fuel element SFEC5, 4378, Pacific Northwest National Laboratory Report PNNL-11438, 1997.
[12] J.J. Katz, E. Rabinowitch, The Chemistry of Uranium – Part I, McGraw-Hill, New York, 1951.
[13] R.B. Smith, The fire properties of metallic uranium (TID-8011), Technical Information Service – Atomic Energy Commission, Wahington DC, 1956.
[14] F. Weigel, in: J.J. Katz, G.T. Seaborg, L.R. Morss (Eds.), The Chemistry of the Actinide Elements, 2nd ed., Chapman and Hall, New York, 1986.
[15] S.L. Robinson, G.J. Thomas, Uranium hydride formation and properties: A Review with commentary on handling

and disposition, Sandia National Laboratory Report SAND96-8206, 1996.
[16] J.L. Stakebake, Chemistry research and development, Research and Development Semi Annual Progress Report, January–June 1977, Rocky Flats Report RFP-2680, 1977.
[17] G.R. Longhurst, Pyrophoricity of tritium-storage bed materials, EG & G Idaho Report EGG-FSP-8050, 1988.
[18] T.C. Totemeier, R.G. Pahl, S.L. Hayes, S.M. Frank, Metallic uranium ZPPR fuel: Corrosion characteristics and corrosion product oxidation kinetics, Argonne National Laboratory Report ANL-98/11, 1998.
[19] S. Lowell, J.E. Shields, Powder Surface Area and Porosity, Chapman and Hall, New York, 1991.
[20] R.M. Alire, Surface areas of uranium and uranium hydride powders, Los Alamos National Laboratory Report LA-UR-73-188, 1973.
[21] Y.B. Rao, R.B. Yadav, R.N. Swamy, B. Gopalan, S. Syamsundar, J. Therm. Anal. 44 (1995) 1439.
[22] K. Winer, C.A. Colmenares, R.L. Smith, F. Wooten, Surf. Sci. 183 (1987) 67.
[23] R.J. McEachern, P. Taylor, J. Nucl. Mater. 254 (1998) 87.